scientific reports

Check for updates

OPEN

Prognosis and immune infiltration prediction in neuroblastoma based on neutrophil extracellular traps-related gene signature

Yeerfan Aierken[1,2], Kezhe Tan[1,2], Tao Liu[1,2] & Zhibao Lv[1]✉

Neuroblastoma (NB) is a malignant tumor originating from the peripheral sympathetic nervous system and high-risk NB patients have a dismal prognosis. Recent studies have underscored the pivotal role of neutrophil extracellular traps (NETs) in the proliferation, metastasis and immune evasion of cancer. To explore the effect of NETs on NB, we have carried out a systematic analysis and showed several findings in the present work. First, expression profiles along with clinical data were analyzed using the training dataset GSE62564 and 36 NETs-related genes were identified to be significantly associated with overall survival. Following LASSO regression analysis, 11 genes were enrolled to construct the NETs signature, which exhibited a robust predictive capability for overall survival with exhibiting high AUC values within the training set. Validation cohorts confirmed a similar predictive efficacy. Next, NB patients were classified into subgroups based on median risk scores and differentially expressed genes were analyzed. Furthermore, the study performed comprehensive analyses encompassing functional enrichment, immune infiltration and drug sensitivity. Enrichment analysis revealed that the high-risk NBs with high-risk score displayed characteristics of oncogenic malignancy, poor prognosis and immunosuppression. Notably, the risk score exhibited a strong correlation with infiltration levels of various immune cells and the sensitivity to anti-cancer drugs, and was further recognized as an independent prognostic factor for NB patients. In summary, our study elucidates a novel NETs-related gene signature comprising 11 genes, which serves a reliable predictor for NB prognosis.

Keywords Neuroblastoma, Neutrophil extracellular traps, Prognosis signature, Therapeutic response, Tumor immune microenvironment

Abbreviations

NB	Neuroblastoma
TANs	Tumor-associated neutrophils
NETs	Neutrophil extracellular traps
DEGs	Differentially expressed genes
SCLC	Small cell lung cancer
ccRCC	Clear cell renal cell carcinoma
GEO	Gene Expression Omnibus
TIME	Tumor immune microenvironment
INSS	International Staging System
COGs	Children's Oncology Groups
LASSO	Least Absolute Shrinkage and Selection Operator
AUC	Area under the curve
GO	Gene Ontology
KEGG	Kyoto Encyclopedia of Genes and Genomes
GSEA	Gene set enrichment analysis
ssGSEA	Single-sample gene set enrichment analysis
TS	Training set

[1]Department of General Surgery, Shanghai Children's Hospital, School of Medicine, Shanghai Jiao Tong University, Shanghai 200062, China. [2]Yeerfan Aierken, Kezhe Tan and Tao Liu contributed equally to this work. ✉email: zhibaolyu@163.com

IVS	Internal validation set
EVS	External validation set
PPI	Protein–protein interaction
FDR	False discovery rate
LRS	LASSO risk scores
OS	Overall survival
ROC	Receiver operating characteristic
TP	Ture-positive
FP	False-positive
ESTIMATE	Estimation of stromal and immune cells in malignant tumor tissue using expression data
TIDE	Tumor immune dysfunction and exclusion
GDSC	Genomics of Drug Sensitivity in Cancer
IC50	Inhibitory concentration 50
HR	Hazard ratio
BP	Biological process
CC	Cellular component
MF	Molecular function
NSE	Normalized enrichment score
VGF	Nerve growth factor inducible
ODC1	Ornithine decarboxylase 1
CCNA2	Cell cyclin A2
TERT	Telomerase reverse transcriptase
SYNM	Synemin
EMT	Epithelial-mesenchymal transition
HLA	Human leukocyte antigen

Neuroblastoma (NB) constitutes 8–10% of pediatric cancers and emerges as the foremost common extracranial solid neoplasm in children, with the highest incidence and mortality during infancy[1,2]. The heterogeneity of NB is pronounced, and the prognosis of NB patients displays substantial variability. The Children's Oncology Groups (COGs) classifies NB patients into multiple risk categories, including very low, low, intermediate and high. The classification is based on a constellation of factors such as age, the International Neuroblastoma Staging System (INSS), histology, DNA copy number, MYCN amplification and other characteristics[3,4]. Advances over the last few decades in therapeutic approaches have remarkably improved the prognosis of NB, but less than 40% of high-risk NB patients achieve long-term survival[5,6]. The poor survival rate in the high-risk group underscores the urgent need for novel biomarkers to enhance the current clinical evaluation system. Furthermore, NB is known for its complex genetic and epigenetic landscape, which contributes to its aggressive behavior and resistance to conventional therapies[7]. Recent studies have highlighted the importance of the tumor microenvironment in NB progression, emphasizing the need for a comprehensive understanding of the interactions between tumor cells and their surrounding stromal and immune cells[8].

Tumor-associated neutrophils (TANs) are a subset of neutrophils that infiltrate tumors, often playing a role in tumor development and proliferation in response to signal molecules from tumor and stromal cells within the microenvironment[9]. Neutrophil extracellular traps (NETs) are a complex composed of DNA, histones, and antimicrobial peptides produced by activated neutrophils. These "traps" are capable of ensnaring various pathogens, including bacteria, fungi and viruses, thereby having an important impact on the innate immune response[10]. Despite the role of NETs in pathogen defense, recent studies have demonstrated that cancer cells can exploit TANs and NETs to further promote tumor progression within the tumor microenvironment[11]. For instance, NETs can encapsulate tumor cells, shielding them from destruction in the bloodstream and facilitating metastasis[11]. This immune evasion mechanism contributes to the poor prognosis observed in different cancer patients. Understanding the interplay between TANs, NETs, and NB is vital for developing new therapeutic strategies and improving patient outcomes. Additionally, TANs have been shown to promote tumor angiogenesis, invasion, and metastasis through the release of various cytokines, chemokines, and proteases[12]. The formation of NETs within the tumor microenvironment has been implicated in creating a pro-tumorigenic niche that supports tumor cell survival and proliferation[13]. Moreover, NETs can interact with other immune cells, such as macrophages and dendritic cells, further modulating the immune response and contributing to tumor immune evasion[14]. A few studies concerning lung cancer and head and neck cancer investigate the prognostic significance of NETs in cancer patients[15–17]. nonetheless, the prognostic impact of NETs-related genes in NB patients remains to be elucidated.

The purpose of this study was to conduct a comprehensive analysis of biomarkers related to NETs and build a NETs-associated risk model to predict and assess the prognosis, tumor-associated immune milieu and immunotherapy response in NB patients, and thus illuminating new perspectives and more evidence on enhancing the NB prognosis and unveiling the potential molecular mechanism of NETs in NB development.

Results

Identification and functional enrichment analysis of NETs-related DEGs in NB

The detailed workflow of our study is shown in (Fig. 1). We obtained expression profiles along with clinical characteristics of 498 NB patients from GSE62564. A total of 36 NETs-related DEGs were identified based on the cutoff criteria of |log2 (fold change) |> 1.0 and an FDR < 0.05 from a pool of 607 NETs-related genes (Fig. 2A). Among these, volcano plot and heatmap demonstrated that 13 NETs-related DEGs were significantly

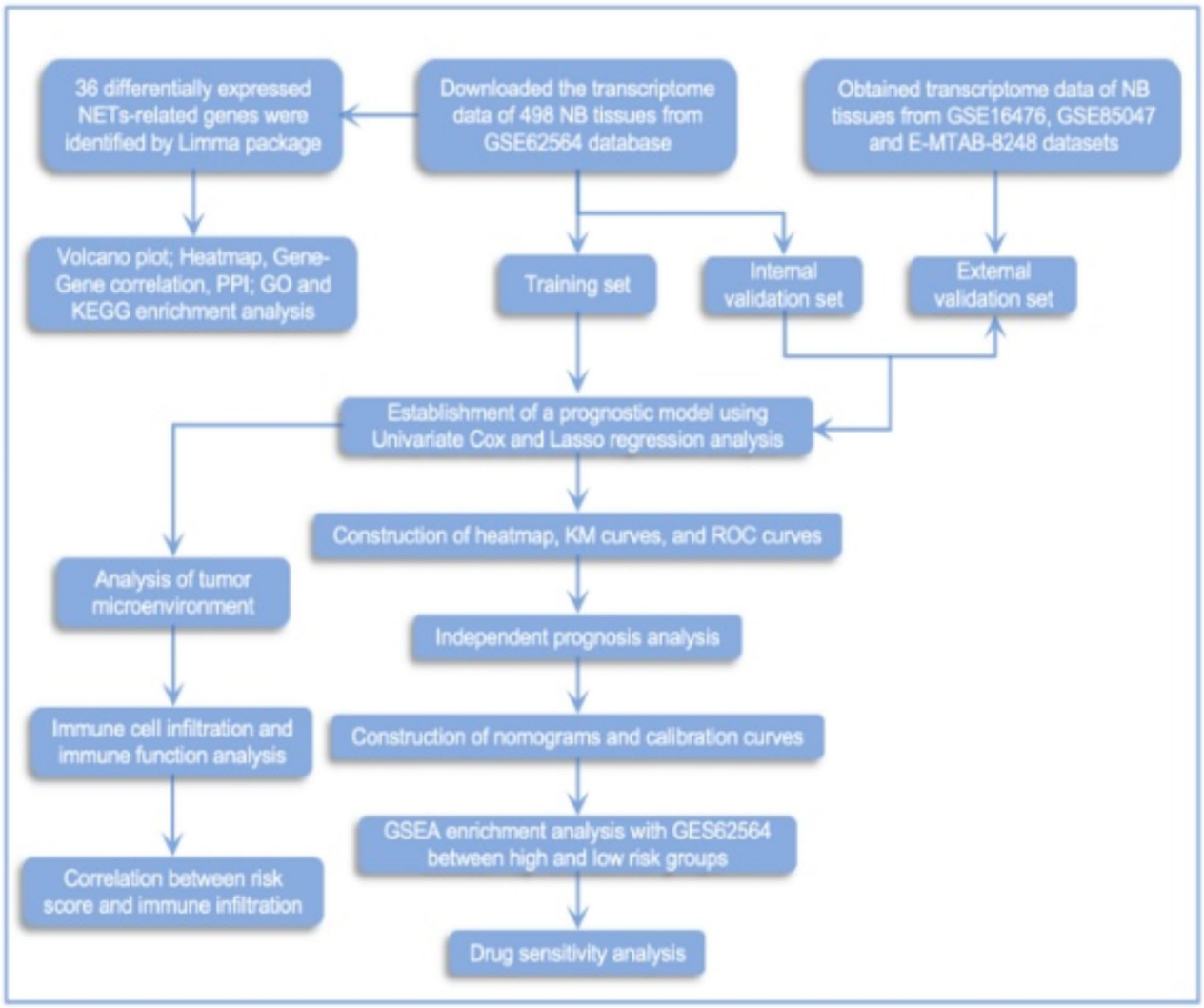

Fig. 1. The flowchart of our research process.

upregulated, whereas 23 NETs-related DEGs were downregulated (Fig. 2B, C). We also showed the correlations among these 36 NETs-related DEGs (Supplementary Fig. 1A).

To obtain a comprehensive overview of these 36 NETs-related DEGs, we engaged both the GeneMANIA and STRING databases in combination with Cytohubba plugin to uncover the gene–gene links, PPI pairs and hub genes among the 36 genes. As demonstrated in Fig. 2D and F, gene–gene and protein–protein interactions of these NETs-related DEGs showed complicated interactions, highlighting hub genes including MMP9, ITGB2, CCNA2, TYMS, FOXM1, SLC18A2, S100B, C3, PTPRC and IL18 using the "MCC" approach (Fig. 2G). Interestingly, TERT, MKI67 and KRT19 were considered as hub genes using the "DMNC" and "MNC" approaches (Supplementary Fig. 1B, C). These 36 genes were subsequently included in GO and KEGG enrichment analyses to further explore the potential functions of the NETs-related DEGs, revealing significant enrichment in GO terms related to "regulation of leukocyte mediated immunity", "granulocyte activation", "neutrophil activation", "exocytic vesicle" and "lyase activity" and in KEGG terms related to "human T-cell leukemia virus 1 infection", "legionellosis" and "estrogen signaling pathway" (Fig. 2E). These results suggest that these NETs-related DEGs are involved in modulating extracellular substance composition and human immune system.

Establishment of a prognostic signature related to NETs

To elucidate the relationship between NETs-related DEGs and survival outcomes within the training set, we performed univariate Cox regression to assess their prognostic relevance. We found that all of the genes exhibited significant prognostic correlations ($P < 0.05$) (Fig. 3A). Based on these 36 NETs-related DEGs, a prognostic signature comprised of 11 NETs-related DEGs (NETs signature) was further established using the LASSO regression (Fig. 3B, C). The LASSO risk scores (LRS) was calculated employing coefficients obtained from the LASSO algorithm (Supplementary Fig. 1D, LRS = − 0.04149xACHE + 0.00858xASCL1 + 0.33793xCCNA2 + 0.00212xFEV + 0.08851xHAPLN4 + − 0.08263xMMP9 + 0.05800xNCAN + 0.15105xODC1 + − 0.20217xSYNM + 0.43015xTERT + 0.13926xVGF). Then, NB patients within both TS and IVS were categorized into low- and

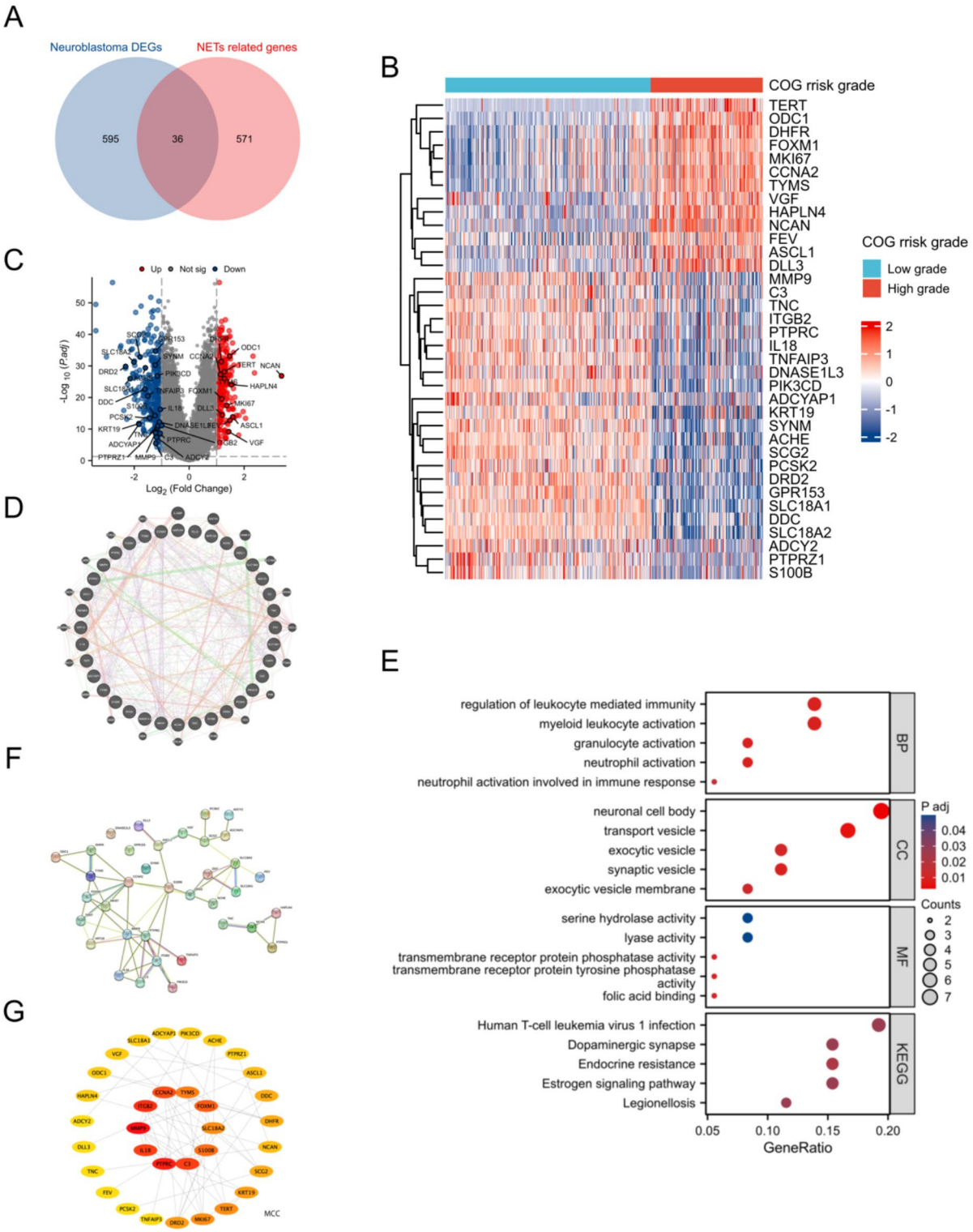

Fig. 2. Differentially expressed NETs-related genes between COG Low grade and High grade in NB tissues. (**A**) A Venn diagram of GSE62564 DEGs and NETs-related genes. (**B**) Heatmap of NETs-related DEGs, with red indicating high expression, and blue indicating low expression. (**C**) Volcano plot indicates NETs-related DEGs, with red dots indicating high expression and blue dots indicating low expression. (**D**) Thirty-six NETs-related DEGs in the GeneMANIA network. (**E**) GO and KEGG analysis of NETs-related DEGs. (**F**) The protein–protein interaction (PPI) networks show the interaction of NETs-related DEGs (interaction score = 0.4). (**G**) Thirty-six NETs-related DEGs in the PPI network were calculated by MCC. NETs: Neutrophil extracellular traps. DEGs: Differentially expressed genes. GO: Gene Ontology. KEGG: Kyoto Encyclopedia of Genes and Genomes.

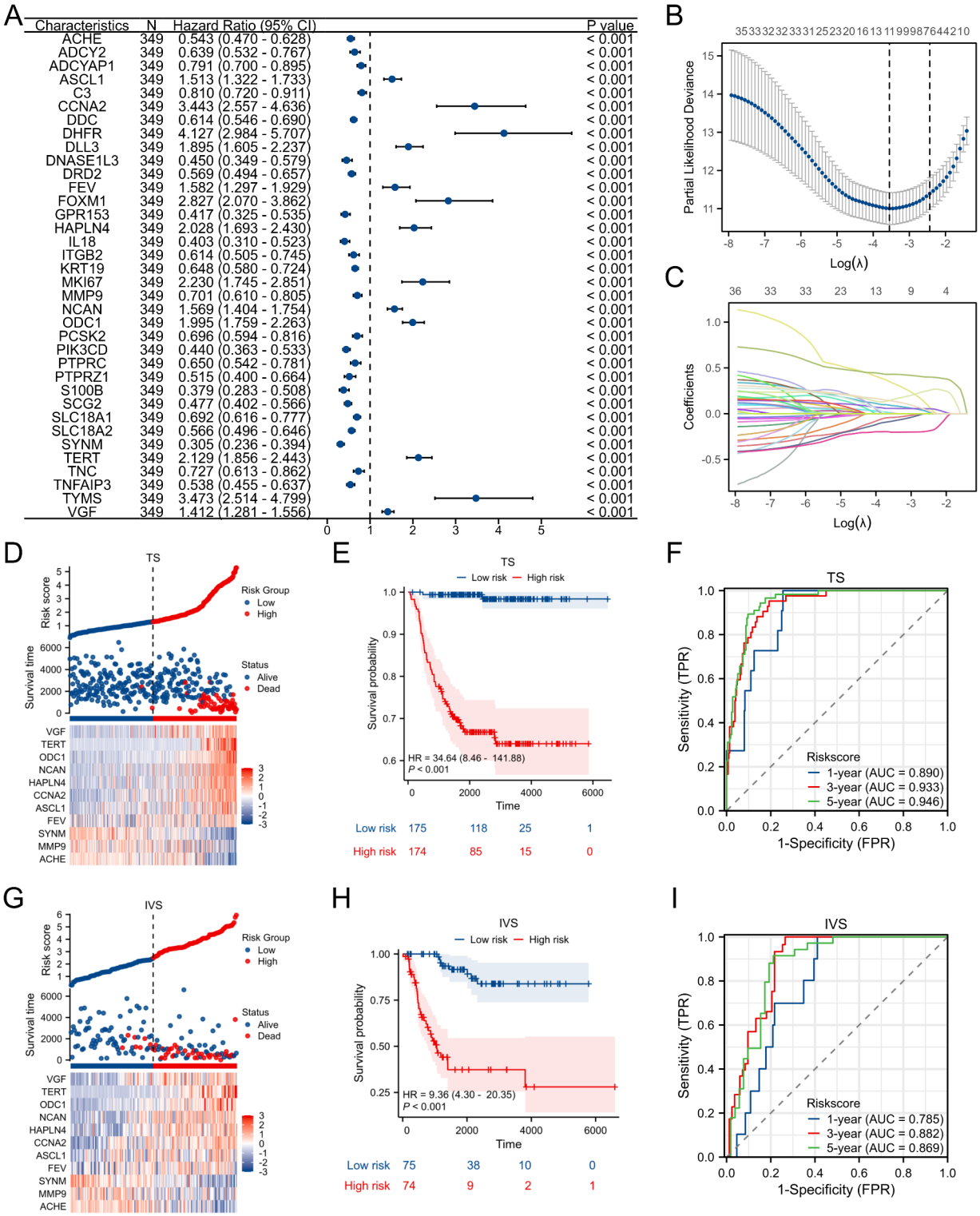

Fig. 3. Eleven-gene prognostic signature based on 36 NETs-related DEGs. (**A**) Univariate Cox regression showing HR and *P* values of 36 NETs-related DEGs. (**B**) LASSO regression screen in TS shows 11 of 36 candidate genes at the least deviance. (**C**) LASSO regression screen in TS shows coefficients of genes at different λ levels. (**D**, **G**) Risk curves, Scatter plots, and heatmaps in TS (**D**) and IVS (**G**). (**E**, **H**) Kaplan–Meier curve of TS (E) and IVS (H) between the low-risk and high-risk groups determined by the 11-gene prognostic signature. (**F, I**) Time-dependent ROC curve in TS (**F**) and IVS (**I**) for 11-gene-based risk score. NETs: Neutrophil extracellular traps. DEGs: differentially expressed genes. HR: hazard ratio. TS: training set. IVS: internal validation set. AUC: area under curve.

high-risk groups based on the median LASSO risk scores (LRS). The risk curve, scatter plots and heatmaps show distinct separation between the low-risk and high-risk groups, indicating that the risk score effectively stratifies patients based their survival outcomes (Fig. 3D, G). Meanwhile, the high-risk group had significantly worse overall survival (OS) than the low-risk group in both TS and IVS (Fig. 3E, H). ROC curve analyses of the prognostic risk score at 1, 3, and 5 years were performed to test the predictive efficiency of the risk signature. The AUC values were robust, with the TS showing AUCs of 0.890, 0.933, and 0.946 for 1-year, 3-year, and 5-year survival predictions, respectively. Similarly, the IVS demonstrated AUCs of 0.785, 0.882, and 0.869 for the same time points (Fig. 3F, I). Additionally, three external datasets (E-MTAB-8248, GSE16476, and GSE85047) were analyzed to validate the applicability of the NETs signature across diverse NB cohorts. We found that the 11-gene prognostic signature exhibited robust performance as evidenced by risk plots (Supplementary Fig. 2A, D, G), Kaplan–Meier curves (Supplementary Fig. 2B, E, H), and ROC curve analyses (Supplementary Fig. 2C, F, I).

The NETs signature is an independent prognostic indicator for NB

To verify whether the calculated risk score and clinical parameters could serve as independent predictors of prognosis, we performed univariate and multivariate Cox analyses within the GSE62564 dataset. We incorporated five clinical variables of NB patients including age, gender, MYCN status, INSS stage, and the risk score into Cox regression analysis. The univariate analysis identified that gender and INSS stage 2 ($P > 0.05$) were not risk factors, in contrast to INSS stage 3, 4 as well as 4S, age, MYCN status and the risk score (HR > 1, $P < 0.05$; Fig. 4A). Multivariate Cox regression analyses revealed that MYCN status was not a risk factor ($P > 0.05$); however, the risk score (HR = 2.008, $P < 0.001$; Fig. 4B) was still a risk factor, similar to the well-established INSS stage 4 (HR = 17.841, $P < 0.005$; Fig. 4B), indicating that the risk score was an independent prognostic factor for OS in patients with NB. We also analyzed the association between the risk score and the clinical parameters, suggesting significant differences between the risk score and the following clinical features: age (< 18 months vs ≧18 months, $P < 0.001$), progression (No vs Yes, $P < 0.001$), MYCN status (Not amplified vs Amplified, $P < 0.001$), and INSS stage (T4 vs T1, T4 vs T2, T4 vs T3, T4 vs T4S, $P < 0.001$) (Supplementary Fig. 1E-H).

Furthermore, a nomogram of clinical prediction integrating age, INSS stage and the risk score was developed to provide a quantitative tool for clinicians to predict 1-, 3- and 5-year OS probabilities for NB patients (Fig. 4C) with excellent agreement shown by the calibration plot (Fig. 4D). The nomogram's predictive accuracy was conducted through ROC analysis, yielding AUC values of 0.863, 0.923 and 0.933 for 1-year, 3-yearand 5-year survival, respectively (Fig. 4E). In addition, the ROC curves substantiated the enhanced predictive capability of the nomogram when combined with additional clinical data (Fig. 4F). DCA for 1-, 3- and 5-year survival highlighted the nomogram's considerable net benefit in survival prediction among NB patients (Fig. 4G–I).

Biological function analysis between low- and high-risk groups

To better understand the biological characteristics of NB in the newly developed prognostic signature, we employed this signature to classify NB patients into low- and high-risk groups based on the median LASSO risk scores (LRS) before using GSEA to investigate GO terms and enriched pathways. The GSEA results indicated significant GO enrichment items including cell cycle checkpoint signaling, DNA replication, DNA repair complex, regulation of cell cycle phase transition and DNA damage sensor activity in the high-risk group (Fig. 5A). Conversely, the low-risk group exhibited enhanced enrichment in chemokine activity, extracellular matrix binding, immune receptor activity, T cell receptor binding and neutrophil-mediated immune responses (Fig. 5B). Pathway analysis highlighted enrichment in the DNA repair pathway full network, extension of telomeres, telomere maintenance, cell cycle mitosis and cellular response to starvation in the high-risk group (Fig. 5C). On the contrary, pathways such as cell adhesion molecules cam, generation of second messenger molecules, T cell receptor signaling pathway, extracellular matrix organization and chemokine signaling pathway were significantly enriched in the low-risk group (Fig. 5D). Furthermore, enrichment analysis of HALLMARKS gene sets was conducted simultaneously, showing somewhat similarity with GSEA in GO terms and pathways. The high-risk group was characterized by enrichment in gene sets of E2F targets, G2/M checkpoint and DNA repair—critical in cell cycle regulation and tumorigenesis (Fig. 5E). In contrast, the inflammatory response, complement and interferon-gamma responses, primarily related to immune cells and cytokines, were activated in the low-risk group (Fig. 5F). These distinctions between risk groups indicated that high-risk group may rely more heavily on these processes, which mostly included DNA damage, DNA repair, cell cycle etc., to sustain their rapid proliferation and survival, potentially contributing to their more aggressive clinical behavior. However, enrichment pattern like immune pathways suggests that low-risk neuroblastomas may be more susceptible to immune surveillance and may have a more robust anti-tumor immune response, which could contribute to better patient outcomes.

TIME analysis of the NETs signature

The TIME has a significant impact on tumor development. This study investigated the relationship between NETs signature and TIME in NB patients using ESTIMATE and ssGSEA algorithms. Our findings indicated that the high-risk group presented elevated stromal , immune and ESTIMATE scores compared to the low-risk group, implicating a compromised TIME conducive to unfavorable clinical outcomes (Fig. 6A–C). Next, the ssGSEA revealed a significant reduction in multiple anti-tumor immune cell types, including both innate immune cells (eosinophils, macrophages, monocytes, NK cells, neutrophils and plasmacytoid dendritic cells) and adaptive immune cells (activated B cells, type 1T helper cells, Type 17 helper cells and T follicular helper cells) in the high-risk group (Fig. 6D–F). Also, an analysis of immune function alterations between risk groups showed predominant downregulation of immune functions in the high-risk group, except CCR, para-inflammation and Type I IFN response (Fig. 7A, B). Furthermore, an examination of 40 immune checkpoints revealed significantly increased expression levels in the low-risk group, establishing an association with the risk

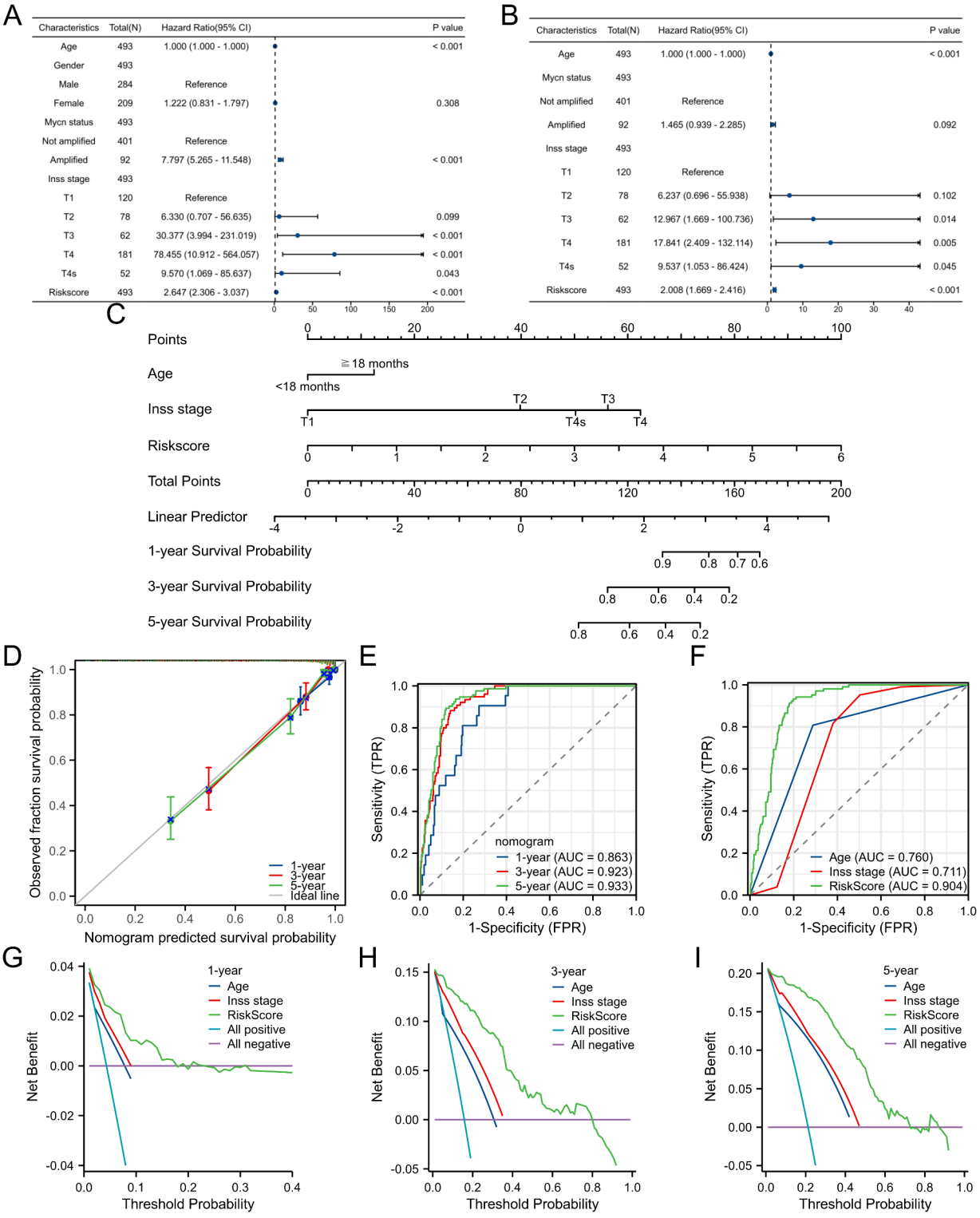

Fig. 4. Nomogram construction in the GSE62564 dataset. (**A**) Univariate Cox regression for age, gender, MYCN status, INSS stage, and risk score. (**B**) Univariate Cox regression for age, MYCN status, INSS stage, and risk score. (**C**) Nomogram predicting survival of NB patients. (**D**) Calibration plot for the nomogram. (**E**) Time-dependent ROC curves at separately one year, three years, and five years. (**F**) ROC curve analysis shows the AUC of age, INSS stage, and risk score. (**G**, **H**, **I**) Decision curve analysis (DCA) for 1, 3, and 5 years. HR: hazard ratio. AUC: area under curve. $P<0.05$ was shown as *, $P<0.01$ as ** and $P<0.001$ as ***.

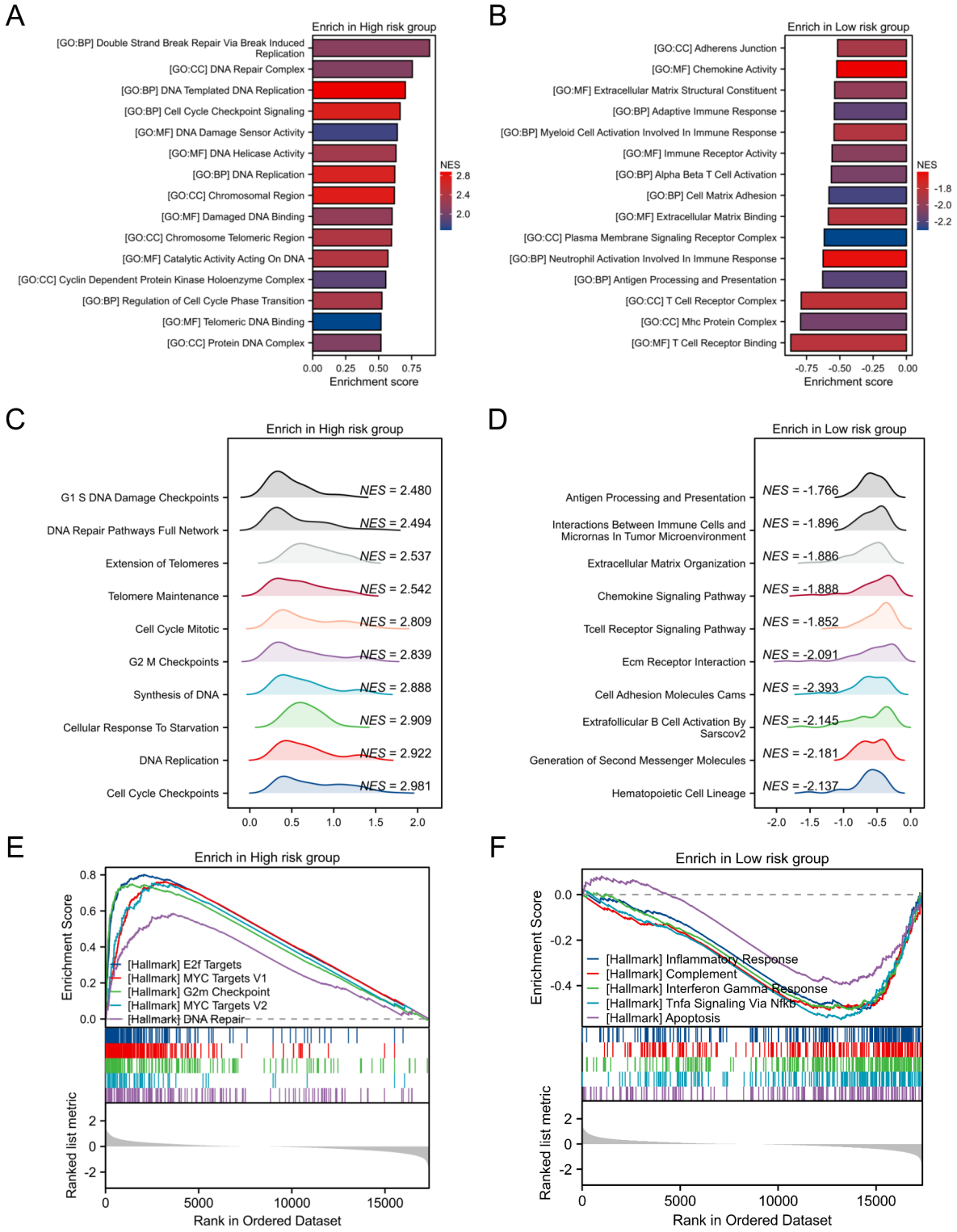

Fig. 5. Enrichment analysis between patients with low- and high-risk scores in the GSE62564 dataset. (**A**, **B**) GSEA function enrichment of the signature based on "oncology" gene sets. (**C**, **D**) GSEA pathway enrichment of the signature based on "curated" gene sets. (**E**,**F**) GSEA analysis of the signature based on "Hallmark" gene sets. GSEA: gene set enrichment analysis. GO: gene oncology. BP: biological process. CC: cellular component. MF: molecular function. NSE: normalized enrichment score.

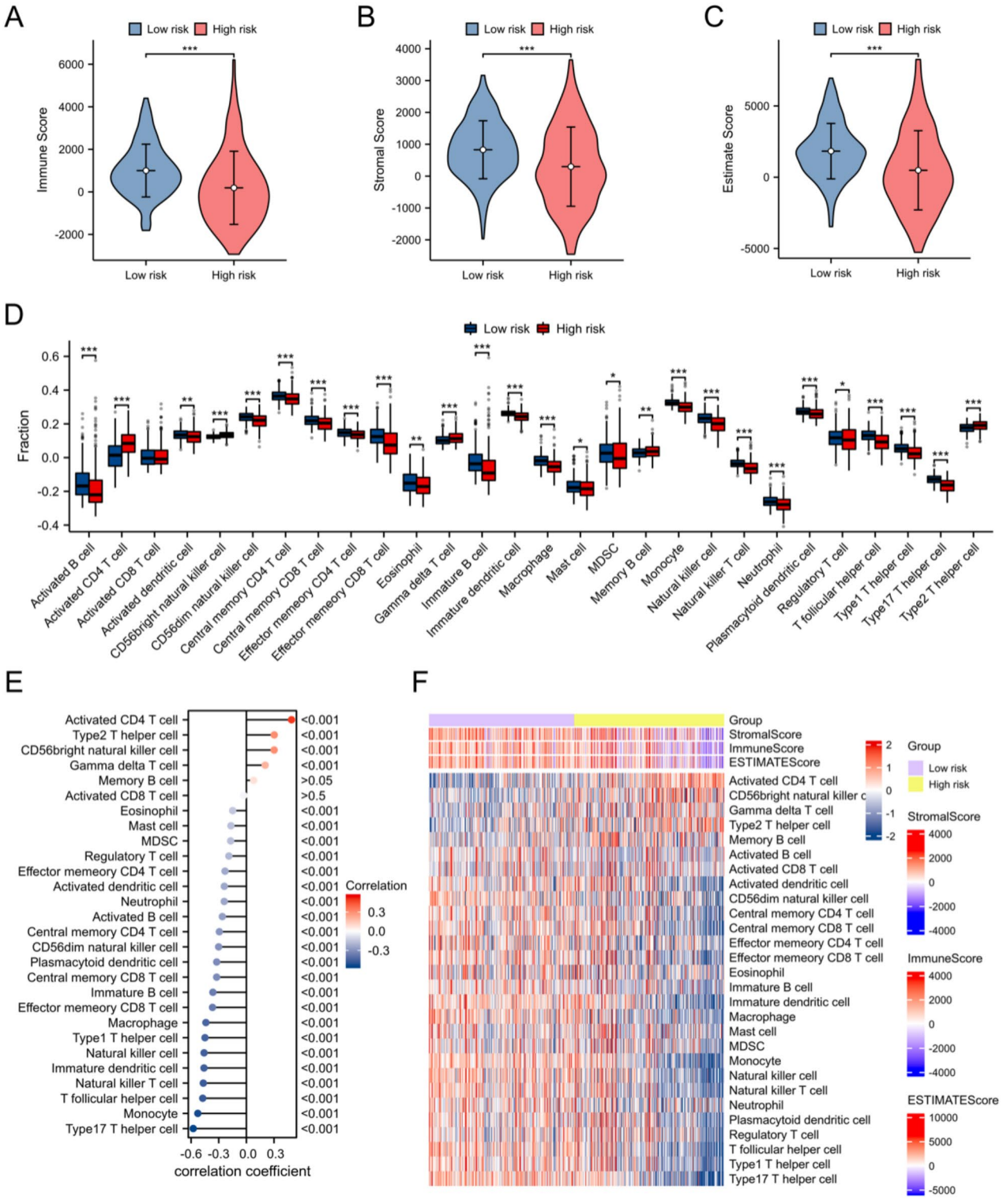

Fig. 6. Immune infiltration analysis at different NETs-related risk subgroups. (**A–C**) The Immune score, Stromal score, and ESTIMATE score between low- and high-risk groups. (**D**) Comparison between low-and high-risk groups of 28 immune cells based on ssGSEA. (**E**) Correlation analysis of NETs-related risk score and immune infiltration. (**F**) Expression heatmap of 28 infiltrating immune cell types in two risk groups. ssGSEA: single sample gene set enrichment analysis. NETs: Neutrophil extracellular traps. $P < 0.05$ was shown as *, $P < 0.01$ as **, and $P < 0.001$ as ***.

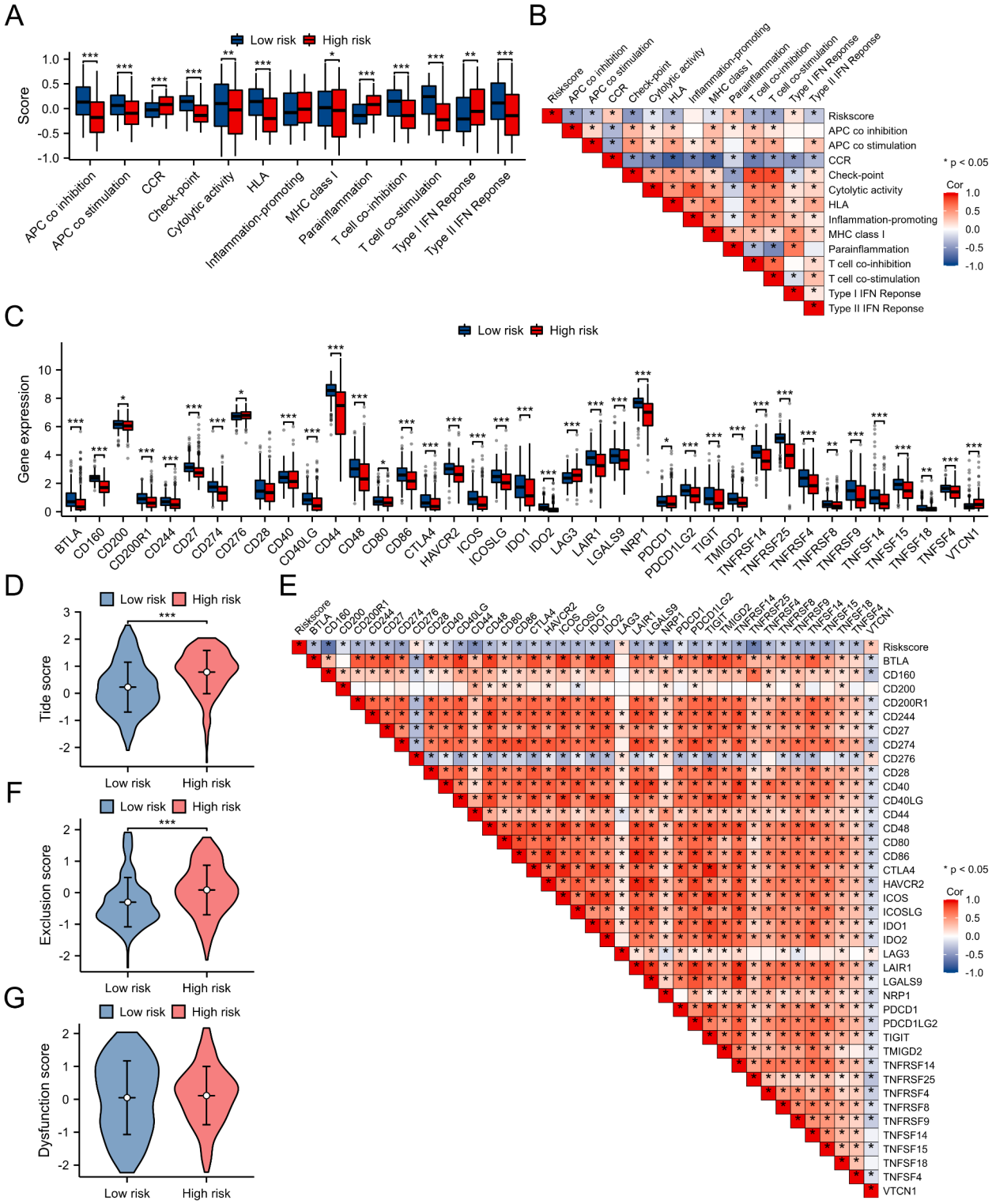

Fig. 7. Immunotherapy response analysis at different NETs-related risk subgroups. (**A**) Comparison of immune function in the low-and high-risk group. (**B**) Heatmap of correlation between 13 immune functions and risk score. (**C**) The expression level of immune checkpoint genes in two risk groups. (**E**) Heatmap of correlation between immune checkpoint genes and risk score. (**D**, **F**, **G**) TIDE, T cell exclusion, and T cell dysfunction score in two risk groups. NETs: Neutrophil extracellular traps. $P<0.05$ was shown as *, $P<0.01$ as ** and $P<0.001$ as ***.

score (Fig. 7C, E). Finally, we applied the tumor immune dysfunction and exclusion score (TIDE) to calculate the immune escape possibility and found that the high-risk group was more susceptible to immune evasion (Fig. 7D, F, G). Collectively, these findings underscore a dichotomy between an immunosuppressive state in the high-risk group and an immune-activated state in the low-risk group, the latter displaying a potentially enhanced response to immunotherapy.

Drug sensitivity analysis

The oncoPredict package was utilized to predict the IC50 of various chemotherapeutic agents for NB patients stratified by different risk groups (Fig. 8). It was observed that IC50 estimated values were significantly lower in high-risk group such as GW843682X and BI-2536 (PLK inhibitor), Dinaciclib (CDK inhibitor), SN-38 and Camptothecin (Topo I inhibitor), Gemcitabine (nucleoside antimetabolite), Sepantronium bromide (survivin inhibitor), TW 37 (Bcl-2 inhibitor), Trichostatin A and Panobinostat (HDAC inhibitor), Bortezomib (proteasome inhibitor), Rapamycin and Dactolisib (mTOR inhibitor) as well as Paclitaxel (tubulin stabilizer). These findings suggest that high-risk NB patients might derive considerable therapeutic benefits from these drugs.

Discussion

NB is the most prevalent extracranial tumor in children, accounting for 15% of pediatric cancer-related fatalities[6]. The notable heterogeneity of NB leads to a wide variation in patient prognoses, thereby limiting the effectiveness of existing therapeutic approaches[18]. Therefore, it underscores the imperative need for innovative prognostic indicators to improve the prognosis of NB patients. The utilization of bioinformatic methodologies presents an innovative strategy for evaluating the prognosis of patients with NB. NETs is a newly discovered type of programmed cell death exclusively triggered by neutrophils. The role of NETs in innate immunity, inflammation and their association with tumor growth, invasion, metastasis and immune evasion of tumor cells has garnered extensive investigation[19–21]. To illustrate, Cools-Lartigue J et al. revealed that NETs has the potential to enhance hepatic metastasis by promoting the survival and proliferation of lung cancer cells[22]. Neutrophil-derived MMP-9 has exhibited a robust correlation with VEGF activation and angiogenesis, which are generally hallmarks of clear cell renal cell carcinoma (ccRCC)[23]. Additionally, the presence of NETs in serum also indicates liver metastases in early-stage breast cancer[24]. Nevertheless, the relationship between NETs signature and the prognosis of individuals with NB remains uncertain. To our knowledge, this is the first study to use RNA-seq data to investigate the predictive significance of NETs signature in NB and their correlation with the immune microenvironment.

Our Study conducted a series of comprehensive analyses and validations to investigate the prognostic biomarkers of NB and build a prognostic signature. We finally developed a prognostic NETs signature and nomogram for NB patients with 11 NETs-related genes, which serves significant utility in enhancing the prognostication and diagnostic processes across diverse NB cohorts. The NETs risk score was proved to be strongly correlated with OS, clinicopathological parameters, immune infiltration and the response to antitumor drugs.

The screened NETs-related 11 genes including ACHE, ASCL1, CCNA2, FEV, HAPLN4, MMP9, NCAN, OCD1, SYNM, TERT and VGF have also been mentioned in other cancer studies to varying degrees. Among these, VGF (nerve growth factor inducible) is highly enriched in NETs, including NB and small cell lung cancer (SCLC). In lung cancer patients, suppressing VGF reduces tumor development by increasing cancer cell apoptosis, and high VGF expression also contributes to chemotherapy treatment resistance and predicts poor survival[25]. ODC1 (ornithine decarboxylase 1), a crucial rate-limiting enzyme in polyamine production, has been identified as a critical determinant of MYCN in oncogenesis. By suppressing ODC1, the impact of MYCN on the initiation and progression of tumors can be diminished[26,27]. Multiple research investigations have demonstrated that CCNA2, also known as Cell Cyclin A2, has the potential to augment cancer aggressiveness, metastasis, and resistance to chemotherapy[28,29]. Due to its effects on angiogenesis, vascularization, epithelial-mesenchymal transition (EMT), proliferation, inflammatory factors and immune response, TERT (telomerase reverse transcriptase) may be an independent prognostic marker for poor survival in human cancer patients[30,31]. Moreover, SYNM (synemin), in contrast to the previously mentioned genes, was markedly downregulated in NB patients. Type IV intermediate filament SYNM is thought to control biological functions like cell adhesion and motility. Our results are consistent with reports that SYNM is positively correlated with a better prognosis in ovarian cancer, while its hypomethylation is linked to aggressiveness in breast cancer[32,33]. The remaining genes, NCAN, MMP9, HAPLN4, FEV, ASCL1 and ACHE have been identified as prognostic indicators in a variety of cancers[34–38]. However, further investigation is necessary to validate each of these genes.

In our study, the identification of specific enriched terms related to NETs is biologically plausible and consistent with the current understanding of NET biology. The enriched terms such as "regulation of leukocyte-mediated immunity" and "granulocyte activation" are directly relevant to the formation and function of NETs, as these processes are essential for neutrophil activation and the subsequent release of NETs[10,11]. Additionally, the involvement of pathways like "human T-cell leukemia virus 1 infection" may reflect the broader role of NETs in modulating the immune response to pathogens and tumor cells, as NETs can capture and neutralize various pathogens, including viruses[10]. The "estrogen signaling pathway" enrichment is particularly intriguing, as recent studies have shown that estrogen can influence neutrophil function and NET formation, potentially through the regulation of neutrophil survival and activation[20]. This finding suggests that hormonal factors may modulate the NET-mediated immune response in the tumor microenvironment. Moreover, the significant enrichment of pathways related to cell cycle regulation and immune response suggests distinct biological behaviors between low- and high-risk neuroblastoma groups which were classified based on the median LASSO risk scores (LRS). For instance, high-risk patients showed alterations in DNA repair and cell cycle checkpoint signaling, which correlate with increased tumor aggressiveness, while low-risk patients exhibited enhanced immune receptor

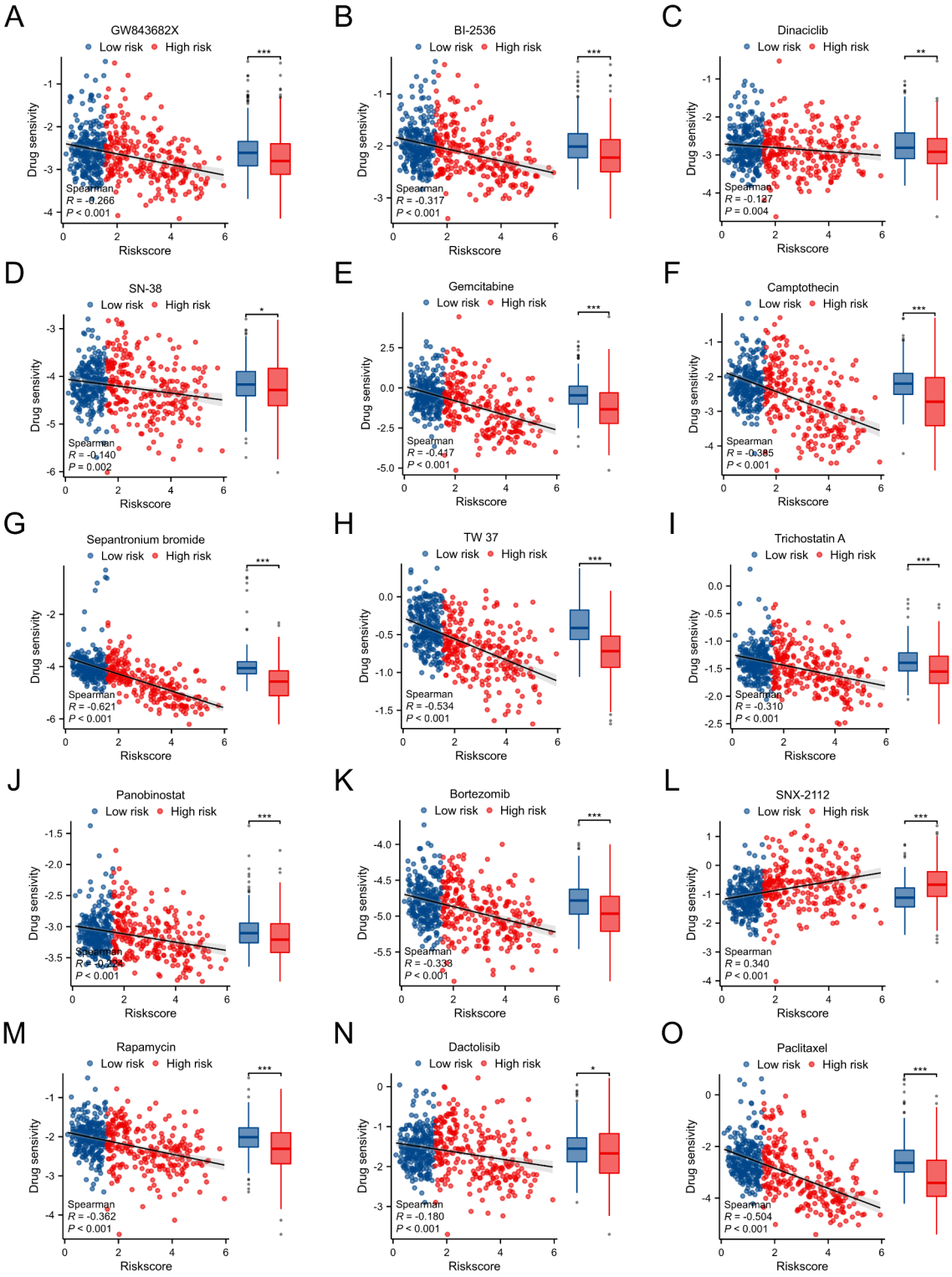

Fig. 8. Evaluation of drug susceptibility between low-and high-risk groups in the GSE62564 dataset. (**A**) GW843682X. (**B**) BI-2536. (**C**) Dinaciclib. (**D**) SN-38. (**E**) Gemcitabine. (**F**) Camptothecin. (**G**) Sepantronium bromide. (**H**) TW 37. (I) Trichostatin A. (**J**) Panobinostat. (**K**) Bortezomib. (**L**) SNX-2112. (**M**) Rapamycin. (**N**) Dactolisib. (**O**) Paclitaxel. $P<0.05$ was shown as *, $P<0.01$ as **, and $P<0.001$ as ***.

activity, suggesting a greater potential for immune evasion. These findings are consistent with other reports indicating that high-risk neuroblastoma is often characterized by dysregulation of cell cycle pathways, which contributes to poor prognosis[39,40]. Thus, understanding these pathways may guide the development of targeted therapies aimed at reprogramming the tumor microenvironment or enhancing the immune response in low-risk patients.

The interplay between immune cells and tumor cells within TIME exerts a considerable impact on the prognosis of patients. Immune cells are an essential part of the TIME and are involved in drug resistance, tumor growth, invasion, metastasis, and antitumor immunity[41]. Besides, recent studies have shown that NETs promote tumorigenesis by preventing tumor cells from interacting with adjacent anti-tumor immune cells[42,43]. Given this, it is imperative to investigate the association between the TIME and NETs risk score. Our analysis indicated that low- and high-risk NB patients exhibited varying immunological profiles and levels of immune cell infiltration. Specifically, activated B cells, CD56dim NK cells, monocytes, macrophages, NK T cells and Type 1 helper cells were positively associated with the low-risk group. Previous research suggests that Th1 cells can play an important role in TME by activating CD8+ T cells and eliciting antitumor effects[44]. In addition, B cells promote humoral immunity and prevent tumor development by secreting immunoglobulins[45]. Similarly, Other cell types such as NK T cells, CD56dim NK cells and macrophages play important anticancer roles in malignancies[46,47]. Our study also found that low-risk patients had considerably higher immune function scores, including checkpoints and HLA, than high-risk patients. The ability of HLA to present antigens to T cells and act as a ligand for receptors on NK cells makes it an important part of innate and adaptive immunity[48,49]. Moreover, high-risk NB patients had lower ESTIMATE and TIDE scores than the low-risk group, indicating that patients in the low-risk group might have an immune 'hot' milieu, allowing them to respond more effectively to immunotherapy. Based on the current findings, we hypothesize that impaired immune cell infiltration and function contribute to the unfavorable prognosis of patients with NB, and these patients can be distinguished by our NETs-related signature.

Additionally, the association between clinical drug sensitivity and the NETs risk score was investigated. The risk score was significantly associated with various chemotherapeutic drugs that regulate the cell cycle, mitosis, apoptosis, DNA replication, chromatin histone acetylation, the PI3K/MTOR signaling pathway, etc. BI-2536 is a cellular pyroptosis-inducing inhibitor of polo-like kinase 1and thus induces cell cycle arrest in the G2/M phase to exert its anticancer effects in various cancer types such as colorectal and ovarian cancers[50,51]. Similarly, the Bcl-2 inhibitor TW 37 promotes cell death by activating the NOTCH-1 signaling pathway in pancreatic cancer[52]. Sepantronium bromide (YM-155) acts as an inhibitor of BIRC5/Survivin and thus specifically inhibits tumor growth and NB cell proliferation both in vitro and in vivo[53]. In high-risk mouse models of NB, the concurrent administration of panobinostat and CBL0137 has been observed to cause chromatin destabilization, interferon activation, augmentation of DNA damage in NB cells, and inhibition of tumor progression[54]. Additionally, Camptothecin and its analogs such as SN22, whose function is defined as a DNA topoisomerase I inhibitor, can lead to rapid tumor regression and lasting therapeutic responses in models of high-risk NB[55]. As suggested by our sensitivity analysis, these medications may have therapeutic potential for NB, warranting further investigation to confirm their efficacy in children with NB.

However, several limitations of our study need to be addressed. Given the retrospective nature of this study, prospective validation is necessary. In addition, the mechanisms underlying the observed crosstalk and interactions within the TIME are not fully elucidated by experiments in this study. Therefore, prospective validation and additional experiments in vivo and in vitro are crucial to substantiate the feasibility of the proposed research directions in future studies.

Conclusion

In conclusion, our study is the first to construct a prognostic signature for NB patients with 11 NETs-related genes, which serves significant utility in enhancing the prognostication and diagnostic processes for patients. The signature was validated across three independent datasets, affirming its robustness. Moreover, the risk score was strongly correlated with OS as well as some clinicopathological characteristics in NB patients. Additionally, the study has delved into the modifications in immune infiltration and the response to antitumor drugs linked to the NETs risk score. The findings of the present study might facilitate our understanding of NB and pave the way for more tailored therapeutic approaches.

Materials and methods

Data source

We selected the NB RNA-seq dataset GSE62564 (n = 498), which had the largest sample size and the most comprehensive clinical as well as survival information, for further analysis. Furthermore, the GSE62564 were randomly divided into a training set (TS, n = 349) and an internal validation set (IVS, n = 149) at a ratio of 7:3. The microarray datasets E-MTAB-8248, GSE16476, and GSE85047 were used as external validation sets (EVS). The above datasets were all obtained from the R2 database (https://hgserver1.amc.nl/cgi-bin/r2/main.cgi/) and normalized by the "Sanger Box" tools (http://sangerbox.com/). The probes and gene symbols were converted according to the platform information of each dataset. After transformation, the GSE62564 dataset had 498 samples and 18409 genes. The GSE16476 dataset had 88 samples and 17905 genes. The E-MTAB-8248 dataset had 223 samples and 19320 genes. The GSE85047 dataset had 283 samples and 13489 genes.

Identification of differentially expressed NETs-related genes

The 607 genes associated with NETs (Supplementary Table 1) were searched in the GeneCards database (https://www.genecards.org/). To identify differentially expressed genes (DEGs) associated with NETs, we conducted

differential analysis on GSE62564 dataset samples between COGs low grade and COGs high grade. The "limma" R package was utilized, and genes were identified as significant DEGs if $|\log2FC| > 1.0$ and $P < 0.05$. After intersecting the DEGs with the NETs genes, a final set of 36 NETs-related DEGs was obtained. The volcano and heatmap of NETs-related DEGs were drawn by using the ggplot2 and ComplexHeatmap R packages separately. Detailed information about the NETs-related DEGs is provided in Supplementary Table 2.

Gene–gene correlation, protein–protein interaction (PPI) network and cytoscape analyses

To gain further insights into the interactions among the DE-GRGs, the gene–gene correlation value was analyzed using the Spearman method. The GeneMANIA tool (https://genemania.org/) was utilized to explore gene–gene networks and functions by applying all accessible online databases and libraries. In addition, protein–protein interactions (PPIs) were plotted using the STRING database (https://string-db.org/), and the minimum interaction score required for PPI analysis was set at 0.4 (medium confidence), after which Cytoscape combined with the Cytohubba plugin was used to visualize the PPI network and hub genes.

Enrichment analysis of NETs-related DEGs and risk score groups

In this study, we employed the "clusterprofiler" R package to conduct Gene Ontology (GO) and Kyoto Encyclopedia of Genes and Genomes (KEGG) pathway enrichment analyses for NETs-related DEGs. The GO analysis is regarded as the gold standard for large-scale functional enrichment studies, as it encompasses diverse biological processes, molecular functions, and cellular components[56]. Moreover, we utilized the KEGG database, which offers comprehensive information regarding genomes, biological pathways, diseases, and drugs[57]. Statistical significance was set at $p < 0.05$ for the GO and KEGG pathways. To identify the underlying mechanism of different outcomes between two risk subgroups (low-risk vs. high-risk), GSEA software (version 4.3.2) was performed to investigate GO terms and the enriched pathways, utilizing c2 (c2.cp.all.v2022.1.Hs.symbols.gmt) and c5 (c5.go.all.v2022.1.Hs.symbols.gmt) from the Molecular Signatures Database (MSigDB). In addition to GO and enriched pathway analysis, a Hallmark gene set (h.all.v2022.1.Hs.symbols.gmt) was also applied. The statistical significance of the screen was set at $P < 0.05$, the false discovery rate (FDR) at $q < 0.25$, and the P-value correction was Benjamini-Hochberg (BH).

Construction of a prognostic signature

Initially, we conducted a univariate Cox regression analysis to evaluate the prognostic significance of NETs-related DEGs in the training set. For this analysis, we utilized the "survival" R package and set the significant filter at 0.05. Subsequently, based on the results obtained from the previous analysis, we employed the "glmnet" R package to create a prognosis signature using LASSO (Least Absolute Shrinkage and Selection Operator). We used tenfold cross-validation (cv.glmnet) to determine the Lasso tuning parameter lambda resulting in the minimum squared error. The 11 most valuable predictive genes and risk score models were obtained based on lambda.min. Then, the 11 genes obtained were integrated into risk profiles, and a risk scoring system was established by utilizing the standardized gene expression values and their corresponding coefficients. The following formula was used to calculate the risk score: risk score = (Expi × bi). (Exp: expression level of the model gene; b: model gene coefficient).

Clinical evaluation of Prognostic signature

All NB patients were classified into low-risk and high-risk subtypes based on the median LASSO risk scores (LRS) in TS, IVS, and EVS. Kaplan–Meier curves depicting overall survival (OS) were generated using the R packages "survminer" and "survival," and the differences between the risk groups were calculated. The "timeROC" and "ggplot2" packages can be used to generate ROC curves and evaluate the predictive performance of the signature for 1-year, 3-year, and 5-year survival probabilities by defining the area under the curve (AUC) values. Additionally, scatter plots and risk curves were constructed to confirm the distribution of risk values among patients in different risk groups and to deduce the risk of NB-associated death. To determine if risk score was an independent prognostic factor for OS in NB patients, univariate and multivariate Cox regression analyses were conducted (package "survival" in R). Covariates included age, gender, INSS stage, and MYCN status. A forest plot was generated using the 'forestplot' package. A nomogram and calibration plot were constructed to investigate the probability of 1-, 3-, and 5-year OS of NB using the package "rms" in R. Furthermore, decision curve analysis was used to determine the clinical usefulness of the signature, and the true-positive (TP) and false-positive (FP) classifications were considered at increasing decision thresholds.

Comprehensive analysis of immune cell infiltration and the tumor immune microenvironment (TIME)

The ESTIMATE R package was used to analyze the abundances of infiltrating stromal and immune cells in NB samples using gene expression data[58]. The ESTIMATE algorithm generates three scores including stromal, immune, and estimate scores. The differences between low- and high-risk groups were compared. We utilized single-sample gene set enrichment analysis (ssGSEA) to measure the sample levels of 28 types of tumor-infiltrating immune cells. The "GSVA" and "GSEABase" R packages are used to calculate differences in 13 immune functions between different risk groups. We predicted immunotherapy outcomes in low- and high-risk groups using the tumor immune dysfunction and exclusion (TIDE) algorithm. Furthermore, the correlation between risk score and immune cells was visualized through the "ggplot2" R package. A heatmap of correlations among risk score, immune checkpoint genes, and 13 immune functions was analyzed using the "corrplot" R package.

Chemotherapy drug sensitivity prediction

We retrieved the dataset of anti-cancer medications from the Genomics of Drug Sensitivity in Cancer (GDSC) website (https://www.cancerrxgene.org/) and employed the "oncoPredict" package to estimate the chemotherapeutic drug sensitivity of NB patients in GSE62564. This package was developed by Maeser et al. for drug sensitivity prediction[59]. The IC50 value serves as a measure of the sensitivity of the chemotherapeutic drug in the cell lines of this cancer type. An elevated IC50 value indicates a reduced sensitivity to the drug, which requires a higher dosage to achieve the desired therapeutic effect. Drugs with median IC50 < 1 were screened, which were considered to be powerful drugs for NB treatment. Finally, differences in response to multiple drugs between the low- and high-risk groups were compared based on the drug sensitivity scores.

Statistical analysis

We used R 4.2.1 for all statistical analyses and visualization. The specific R packages used are described in each section. Normally and nonnormally distributed continuous variables were compared using t-tests and Wilcoxon rank sum tests, respectively. Spearman correlation analysis was used to evaluate correlations between variables, and Kaplan–Meier analysis was used to evaluate survival. P values < 0.05 were considered statistically significant. Additionally, $^{*}P < 0.05$, $^{**}P < 0.01$, and $^{***}P < 0.001$.

Data availability

The datasets generated and analyzed during the current study can be downloaded from public databases including GEO and ArrayExpress: GSE62564: https://www.ncbi.nlm.nih.gov/geo/query/acc.cgi?acc=GSE62564; GSE16476: https://www.ncbi.nlm.nih.gov/geo/query/acc.cgi?acc=gse16476; GSE85047: https://www.ncbi.nlm.nih.gov/geo/query/acc.cgi?acc=gse85047; E-MTAB-8248: https://www.ebi.ac.uk/biostudies/arrayexpress/studies/E-MTAB-8248.

Received: 17 April 2024; Accepted: 29 January 2025
Published online: 13 February 2025

References

1. Siegel, D. A. et al. Cancer incidence rates and trends among children and adolescents in the United States, 2001–2009. *Pediatrics* **134**, e945-955. https://doi.org/10.1542/peds.2013-3926 (2014).
2. Marshall, G. M. et al. The prenatal origins of cancer. *Nat. Rev. Cancer* **14**, 277–289. https://doi.org/10.1038/nrc3679 (2014).
3. Pinto, N. R. et al. Advances in risk classification and treatment strategies for neuroblastoma. *J. Clin. Oncol.* **33**, 3008–3017. https://doi.org/10.1200/jco.2014.59.4648 (2015).
4. Matthay, K. K. et al. Neuroblastoma. *Nat. Rev. Dis. Primers* **2**, 16078. https://doi.org/10.1038/nrdp.2016.78 (2016).
5. Casey, D. L. & Cheung, N. V. Immunotherapy of pediatric solid tumors: Treatments at a crossroads, with an emphasis on antibodies. *Cancer Immunol. Res.* **8**, 161–166. https://doi.org/10.1158/2326-6066.Cir-19-0692 (2020).
6. Lundberg, K. I., Treis, D. & Johnsen, J. I. Neuroblastoma heterogeneity, plasticity, and emerging therapies. *Curr. Oncol. Rep.* **24**, 1053–1062. https://doi.org/10.1007/s11912-022-01270-8 (2022).
7. Bosse, K. R. & Maris, J. M. Advances in the translational genomics of neuroblastoma: From improving risk stratification and revealing novel biology to identifying actionable genomic alterations. *Cancer* **122**, 20–33. https://doi.org/10.1002/cncr.29706 (2016).
8. Rishabh, S. et al. Emerging trends in neuroblastoma dagnosis, therapeutics, and research. *Mol. Neurobiol* **13**, 1. https://doi.org/10.1007/s12035-024-04680-w (2025).
9. Cortez-Retamozo, V. et al. Origins of tumor-associated macrophages and neutrophils. *Proc. Natl. Acad. Sci. USA* **109**, 2491–2496. https://doi.org/10.1073/pnas.1113744109 (2012).
10. Papayannopoulos, V. Neutrophil extracellular traps in immunity and disease. *Nat. Rev. Immunol.* **18**, 134–147. https://doi.org/10.1038/nri.2017.105 (2018).
11. Demkow, U. Neutrophil Extracellular Traps (NETs) in cancer invasion, evasion and metastasis. *Cancers (Basel)* https://doi.org/10.3390/cancers13174495 (2021).
12. Houghton, A. M. The paradox of tumor-associated neutrophils: fueling tumor growth with cytotoxic substances. *Cell Cycle* **9**, 1732–1737. https://doi.org/10.4161/cc.9.9.11571 (2010).
13. Park, J. et al. Cancer cells induce metastasis-supporting neutrophil extracellular DNA traps. *Sci. Transl. Med.* **8**, 361ra138. https://doi.org/10.1126/scitranslmed.aag1711 (2016).
14. Cedervall, J. et al. Neutrophil extracellular traps accumulate in peripheral blood vessels and compromise organ function in tumor-bearing animals. *Cancer Res.* **75**, 2653–2662. https://doi.org/10.1158/0008-5472.CAN-14-3299 (2015).
15. Fang, C. et al. A innovative prognostic symbol based on neutrophil extracellular traps (NETs)-related lncRNA signature in non-small-cell lung cancer. *Aging (Albany NY)* **13**, 17864–17879. https://doi.org/10.18632/aging.203289 (2021).
16. Zhang, Y. et al. A signature for pan-cancer prognosis based on neutrophil extracellular traps. *J. Immunother. Cancer* https://doi.org/10.1136/jitc-2021-004210 (2022).
17. Li, Q. et al. A novel neutrophil extracellular trap signature to predict prognosis and immunotherapy response in head and neck squamous cell carcinoma. *Front Immunol.* **13**, 1019967. https://doi.org/10.3389/fimmu.2022.1019967 (2022).
18. Qiu, B. & Matthay, K. K. Advancing therapy for neuroblastoma. *Nat. Rev. Clin. Oncol.* **19**, 515–533. https://doi.org/10.1038/s41571-022-00643-z (2022).
19. Tan, C., Aziz, M. & Wang, P. The vitals of NETs. *J. Leukoc Biol.* **110**, 797–808. https://doi.org/10.1002/JLB.3RU0620-375R (2021).
20. Shahzad, M. H. et al. Neutrophil extracellular traps in cancer therapy resistance. *Cancers (Basel)* **14**, 1359. https://doi.org/10.3390/cancers14051359 (2022).
21. Chen, Y. et al. The role of neutrophil extracellular traps in cancer progression, metastasis and therapy. *Exp. Hematol. Oncol.* **11**, 99. https://doi.org/10.1186/s40164-022-00345-3 (2022).
22. Cools-Lartigue, J. et al. Neutrophil extracellular traps sequester circulating tumor cells and promote metastasis. *J. Clin. Invest.* **123**, 3446–3458. https://doi.org/10.1172/JCI67484 (2013).
23. Li, R., Jiang, X., Wang, P. & Liu, X. Prognostic value of neutrophil extracellular trap signature in clear cell renal cell carcinoma. *Front. Oncol.* **13**, 1205713. https://doi.org/10.3389/fonc.2023.1205713 (2023).
24. Yang, L. et al. DNA of neutrophil extracellular traps promotes cancer metastasis via CCDC25. *Nature* **583**, 133–138. https://doi.org/10.1038/s41586-020-2394-6 (2020).
25. Yang, L. H. et al. Neuronal survival factor VGF promotes chemoresistance and predicts poor prognosis in lung cancers with neuroendocrine feature. *Int. J. Cancer* **151**, 1611–1625. https://doi.org/10.1002/ijc.34193 (2022).

26. Qiu, L., Zhou, R., Luo, Z., Wu, J. & Jiang, H. CDC27-ODC1 axis promotes metastasis, accelerates ferroptosis and predicts poor prognosis in neuroblastoma. *Front. Oncol.* **12**, 774458. https://doi.org/10.3389/fonc.2022.774458 (2022).
27. Yang, J. Approval of DFMO for high-risk neuroblastoma patients demonstrates a step of success to target MYC pathway. *Br. J. Cancer* **130**, 513–516. https://doi.org/10.1038/s41416-024-02599-6 (2024).
28. Fischer, M., Quaas, M., Steiner, L. & Engeland, K. The p53–p21-DREAM-CDE/CHR pathway regulates G2/M cell cycle genes. *Nucleic Acids Res.* **44**, 164–174. https://doi.org/10.1093/nar/gkv927 (2016).
29. Zhang, S., Tischer, T. & Barford, D. Cyclin A2 degradation during the spindle assembly checkpoint requires multiple binding modes to the APC/C. *Nat. Commun.* **10**, 3863. https://doi.org/10.1038/s41467-019-11833-2 (2019).
30. Bertorelle, R. et al. Telomerase is an independent prognostic marker of overall survival in patients with colorectal cancer. *Br. J. Cancer* **108**, 278–284. https://doi.org/10.1038/bjc.2012.602 (2013).
31. Liu, M. et al. The regulations of telomerase reverse transcriptase (TERT) in cancer. *Cell Death Dis.* **15**, 90. https://doi.org/10.1038/s41419-024-06454-7 (2024).
32. Kapoor, S. Synemin: An evolving role in tumor growth and progression. *J. Cachexia Sarcopenia Muscle* **5**, 347–348. https://doi.org/10.1007/s13539-013-0122-x (2014).
33. Chen, S. et al. A risk model of gene signatures for predicting platinum response and survival in ovarian cancer. *J. Ovarian Res.* **15**, 39. https://doi.org/10.1186/s13048-022-00969-3 (2022).
34. Nischalke, H. D. et al. A common polymorphism in the NCAN gene is associated with hepatocellular carcinoma in alcoholic liver disease. *J. Hepatol.* **61**, 1073–1079. https://doi.org/10.1016/j.jhep.2014.06.006 (2014).
35. Yang, Q. et al. Candidate Biomarkers and Molecular Mechanism Investigation for Glioblastoma Multiforme Utilizing WGCNA. *Biomed. Res. Int.* **2018**, 4246703. https://doi.org/10.1155/2018/4246703 (2018).
36. Liang, Y. X. et al. Tumor suppressor role and clinical significance of the FEV gene in prostate cancer. *Dis. Markers* **2022**, 8724035. https://doi.org/10.1155/2022/8724035 (2022).
37. Miyakawa, K. et al. ASCL1 regulates super-enhancer-associated miRNAs to define molecular subtypes of small cell lung cancer. *Cancer Sci.* **113**, 3932–3946. https://doi.org/10.1111/cas.15481 (2022).
38. Shaikh, S., Yadav, D. K., Bhadresha, K. & Rawal, R. M. Integrated computational screening and liquid biopsy approach to uncover the role of biomarkers for oral cancer lymph node metastasis. *Sci. Rep.* **13**, 14033. https://doi.org/10.1038/s41598-023-41348-2 (2023).
39. Wang, H., Wang, X., Xu, L. & Zhang, J. TP53 and TP53-associated genes are correlated with the prognosis of paediatric neuroblastoma. *BMC Genom Data* **23**, 41. https://doi.org/10.1186/s12863-022-01059-5 (2022).
40. Rössler, J., Breit, S., Havers, W. & Schweigerer, L. Vascular endothelial growth factor expression in human neuroblastoma: up-regulation by hypoxia. *Int. J. Cancer* **81**, 113–117. https://doi.org/10.1002/(sici)1097-0215(19990331)81:1%3c113::aid-ijc19%3e3.0.co;2-l (1999).
41. Zhou, F. et al. Spatial architecture of regulatory T-cells correlates with disease progression in patients with nasopharyngeal cancer. *Front. Immunol.* **13**, 1015283. https://doi.org/10.3389/fimmu.2022.1015283 (2022).
42. Ireland, A. S. & Oliver, T. G. Neutrophils create an ImpeNETrable shield between tumor and cytotoxic immune cells. *Immunity* **52**, 729–731. https://doi.org/10.1016/j.immuni.2020.04.009 (2020).
43. Teijeira, Á. et al. CXCR1 and CXCR2 chemokine receptor agonists produced by tumors induce neutrophil extracellular traps that interfere with immune cytotoxicity. *Immunity* **52**, 856-871.e858. https://doi.org/10.1016/j.immuni.2020.03.001 (2020).
44. Johnson, A. M. et al. Cancer cell-intrinsic expression of MHC Class II regulates the immune microenvironment and response to Anti-PD-1 therapy in lung adenocarcinoma. *J. Immunol.* **204**, 2295–2307. https://doi.org/10.4049/jimmunol.1900778 (2020).
45. Wang, S. S. et al. Tumor-infiltrating B cells: Their role and application in anti-tumor immunity in lung cancer. *Cell Mol. Immunol.* **16**, 6–18. https://doi.org/10.1038/s41423-018-0027-x (2019).
46. Yuan, Q. et al. Development and validation of a novel N6-methyladenosine (m6A)-related multi- long non-coding RNA (lncRNA) prognostic signature in pancreatic adenocarcinoma. *Bioengineered* **12**, 2432–2448. https://doi.org/10.1080/21655979.2021.1933868 (2021).
47. Nelson, A., Lukacs, J. D. & Johnston, B. The Current Landscape of NKT Cell Immunotherapy and the Hills Ahead. *Cancers (Basel)* **13**, https://doi.org/10.3390/cancers13205174 (2021).
48. Lin, A. & Yan, W. H. The emerging roles of human leukocyte antigen-F in immune modulation and viral infection. *Front Immunol* **10**, 964. https://doi.org/10.3389/fimmu.2019.00964 (2019).
49. Han, J. et al. Assessment of human leukocyte antigen-based neoantigen presentation to determine pan-cancer response to immunotherapy. *Nat. Commun.* **15**, 1199. https://doi.org/10.1038/s41467-024-45361-5 (2024).
50. Huo, J., Shen, Y., Zhang, Y. & Shen, L. BI 2536 induces gasdermin E-dependent pyroptosis in ovarian cancer. *Front Oncol.* **12**, 963928. https://doi.org/10.3389/fonc.2022.963928 (2022).
51. Zhang, Y. et al. Small molecule inhibitors from organoid-based drug screen induce concurrent apoptosis and gasdermin E-dependent pyroptosis in colorectal cancer. *Clin. Transl. Med.* **12**, e812. https://doi.org/10.1002/ctm2.812 (2022).
52. Alam, M. et al. B cell lymphoma 2: A potential therapeutic target for cancer therapy. *Int. J. Mol. Sci.* **22**, 10442. https://doi.org/10.3390/ijms221910442 (2021).
53. Li, X. et al. YM155 inhibits neuroblastoma growth through degradation of MYCN: A new role as a USP7 inhibitor. *Eur. J. Pharm. Sci.* **181**, 106343. https://doi.org/10.1016/j.ejps.2022.106343 (2023).
54. Xiao, L. et al. Dual targeting of chromatin stability by the Curaxin CBL0137 and histone deacetylase inhibitor panobinostat shows significant preclinical efficacy in neuroblastoma. *Clin. Cancer Res.* **27**, 4338–4352. https://doi.org/10.1158/1078-0432.Ccr-20-2357 (2021).
55. Alferiev, I. S. et al. Poloxamer-linked prodrug of a topoisomerase I inhibitor SN22 shows efficacy in models of high-risk neuroblastoma with primary and acquired chemoresistance. *FASEB J* **36**, e22213. https://doi.org/10.1096/fj.202101830RR (2022).
56. The Gene Ontology, C. The Gene Ontology Resource: 20 years and still GOing strong. *Nucleic Acids Res.* **47**, 1330–1338. https://doi.org/10.1093/nar/gky1055 (2019).
57. Kanehisa, M., Furumichi, M., Sato, Y., Kawashima, M. & Ishiguro-Watanabe, M. KEGG for taxonomy-based analysis of pathways and genomes. *Nucleic Acids Res.* **51**, D587–D592. https://doi.org/10.1093/nar/gkac963 (2023).
58. Yoshihara, K. et al. Inferring tumour purity and stromal and immune cell admixture from expression data. *Nat. Commun.* **4**, 2612. https://doi.org/10.1038/ncomms3612 (2013).
59. Maeser, D., Gruener, R. F. & Huang, R. S. oncoPredict: An R package for predicting in vivo or cancer patient drug response and biomarkers from cell line screening data. *Brief Bioinform.* **22**, bbab260. https://doi.org/10.1093/bib/bbab260 (2021).

Acknowledgements

The authors would like to thank the researchers who provided open access to the raw data.

Author contributions

Yeerfan Aierken: Conceptualization, Writing – original draft. Kezhe Tan: Conceptualization, Writing – original draft. Tao Liu: Software, Writing – original draft. Zhibao Lv: Data curation, Writing – review & editing.

Funding
None.

Declarations

Competing interests
The authors declare no competing interests.

Ethics approval
This study does not involve ethical approval.

Additional information
Supplementary Information The online version contains supplementary material available at https://doi.org/10.1038/s41598-025-88608-x.

Correspondence and requests for materials should be addressed to Z.L.